Intelligent Automation And Soft Computing, 2020
Copyright © 2020, TSI® Press
Vol. 26, no.2, 367–383
https://doi.org/10.31209/2020.100000206

A Study of Single Image Haze Removal Using a Novel White-Patch Retinex-Based Improved Dark Channel Prior Algorithm

Yao-Liang Chung[1,*], Hung-Yuan Chung[2], and Yu-Shan Chen[2]

[1] Department of Communications, Navigation and Control Engineering, National Taiwan Ocean University, Keelung City 20224, Taiwan;
[2] Department of Electrical Engineering, National Central University, Taoyuan City 32001, Taiwan;
* Correspondence: ylchung@email.ntou.edu.tw; Tel.: +886-2-2462-2192 (ext. 7224);

ABSTRACT

In this study, we introduce an algorithm which is based on a series of well-known algorithms and mainly uses an improved dark channel prior algorithm and the White-Patch Retinex algorithm (both are heterogeneous algorithms) in order to effectively remove the haze from a single image. When used in conjunction with a heterogeneous architecture, the value of the algorithm becomes even greater. With an effective design and a novel procedure, the proposed algorithm can not only restore a clear image, but also solve the halo effect, color distortion, and long operating time issues resulting from the dark channel prior. Rich experimental results (visually and numerically) confirm that the performance and effectiveness of the new algorithm are better than those of the dark channel prior algorithm, indicating the applicability of the new algorithm.

KEY WORDS: Dark channel prior; haze removal; image restoration; White-Patch Retinex

1 INTRODUCTION

WHILE taking pictures or using instant image devices, we sometimes cannot obtain complete and clear images due to external factors. The incomplete transmission of light is the main reason for such issues. This occurs because there are many kinds of suspended particles in the air, such as hydrometeors, dust, etc., that cause light scattering or refraction in different scenes and climates (Nayar and Narashiman (1999)). Sometimes an image is dark and unclear due to insufficient light; sometimes particulates in the air cause color distortion in an image; and sometimes environmental factors such as haze, rain, fog, etc., will blur or degrade the image quality. Due to the aforementioned conditions, we need to use image dehazing technology to upgrade scene visibility and image quality, and such technology can also be useful for road recognition, self-driving vehicles, drones, and surveillance systems, allowing the avoidance of work stoppages due to blurred images or identification errors.

Studies conducted by Singh and Kumar (2018) and Saggu and Singh (2015) provided a complete overview and survey of haze removal techniques. Typical methods for haze removal can be classified into three categories: (i) histogram equalization, (ii) multiple images dehazing, and (iii) single image dehazing. Histogram equalization (Kim et al. (1998) and Stark (2000)) is based on image processing. This method always loses depth information because only contrast is enhanced; therefore the results are limited and unnatural.

For multiple images dehazing, Narasimhan and Nayar proposed a method of defogging by estimating the brightness of images of two identical scenes under different weather conditions (Narasimhan and Nayar (2003)). Furthermore, other scholars have proposed utilizing the depth information of multiple images (Kopt et al. (2008) and Hautiere et al. (2007)), but this method cannot be used in dynamic image defogging because the information needed cannot be easily retrieved. Shwartz et al. (2006) and Schechner et al. (2001) tried to perform dehazing by using two or more photos with different degrees of polarization; however, the utility of this method is very limited because it requires rotation of the polarizer angle. Mai et al. (2014) used image RGB values as a feature to train back-propagation neural networks for image dehazing. This method, however, first requires

CONTACT Yao-Liang Chung ylchung@email.ntou.edu.tw

creating hazing map transmissions using atmospheric light and other data, which takes considerable time for training. Although all of these methods are helpful for image dehazing, they are not suitable for most cameras because the image acquisition process has a certain degree of difficulty and requires special hardware devices.

For single image dehazing, Fattal (2008) proposed the application of scene reflectance to obtain a solution in which the transmission and shadow are not correlated; however, this method is not suitable in thick haze or when the assumption is not valid. Tan (2008) observed that a sharp image has a higher contrast than a blurred one. Based on this observation, he enhanced the contrast of restored images, but it is easy to generate block artifacts in the deep information-discontinuous zone using this method. He et al. (2011) proposed the dark channel prior algorithm to dehaze hazy images, and their approach was based on a key observation that most local patches in haze-free outdoor images contain some pixels which have very low intensities in at least one color channel. Later, Ji et al. (2014), Shiau et al. (2013), Zhang and Zhao (2017), and El-Hashash et al. (2015) implemented image dehazing by enhancing hardware such as the embedded system or using FPGA as a core processor and associating it with a dehazing algorithm. Nair and Sankaran (2015) divided the image haze into several windows, estimating the window's air-light for each window. Although this method can improve the image inside the window, overall, it is unnatural at the window boundaries.

In addition to the general conditions that cause image blurring, the increasing occurrence of dust pollution has recently become a growing cause of image blurring. For example, on March 21, 2010, dust from northern China caused the sky above Taiwan to stay hazy for an entire day, marking the first and worst dust event in Taiwan (BBC News (2010)). Needless to say, the situation was even more severe in northern China itself. Hazy air makes it impossible for people to make out the details in an image. To address this issue, we aimed to improve image dehazing not just for general foggy images, but also for images affected by dust. In recent years, the dark channel prior algorithm has not only performed well in image dehazing (Meng et al. (2013), Zhu et al. (2015), Lu et al. (2014), Cho et al. (2016), Hsieh et al. (2014), Long et al. (2012), and Hsieh et al. (2016)), but has also had many applications (Hu et al. (2015), Pan et al. (2015), and Wang and Fan (2014)). However, the dark channel prior algorithm still has certain insufficiencies: it can easily create a partial halo effect; it can easily cause color distortions; and the soft matting requires too much time during transmission enhancement.

In this study, we mainly utilize an improved dark channel prior algorithm and the White-Patch Retinex algorithm (which was proposed by Land and McCann (1971)) to address the aforementioned issues and achieve better image dehazing. It should be noted that these two algorithms are heterogeneous. When used in conjunction with a heterogeneous architecture, the value of our algorithm becomes even greater. This paper makes the following contributions:

- This new image dehazing algorithm is based on a series of well-known algorithms and mainly uses the heterogeneous algorithms that are the improved dark channel prior algorithm and the White-Patch Retinex algorithm. Extensive experimental results (visually and numerically) show that the new algorithm is superior to the dark channel prior algorithm in terms of effectiveness and performance.
- The improved dark channel prior algorithm combines the dark channel prior algorithm, a median filter, and a guided image filter. The median filter can eliminate the halo generated at the discontinuous portion of an image edge (compared with a minimum filter, the median filter is better in preserving image edges). The guided image filter is able to smooth image edges. The two filters make the overall image look more harmonious and natural.
- In the image dehazing field, many scholars apply the dark channel prior algorithm, but most of them ignore the fact that different particles in the air will cause the level of absorption and scattering to vary along with varied light frequencies and that failing to make adjustments according to the light frequency will cause color distortion. However, when used in conjunction with the White-Patch Retinex algorithm, the three-color RBG channels can demonstrate a similar distribution and keep the colors unchanged. This allows the image dehazing method that we proposed to be applied to a more diverse range of scenes; it can identify the object and its color in ordinary and dusty weather conditions. As a result, our proposed algorithm can improve image dehazing not just for hazy images in general, but also for images affected by dust.
- This study can speed up the operating speed of image dehazing. The soft matting used to enhance transmission needs to process the complicated matting Laplacian matrix; we use the guided image filter to replace this. The guided image filter is not only less complex in terms of processing but also achieves a dehazing effect which is similar to that of soft matting. There are many digital video systems on the market, such as those used in monitors, those used to make recordings in cars when driving, and those used in self-driving cars and drones. These will serve as important application platforms for emerging technologies associated with fifth generation (5G) cellular network

systems (Gupta and Jha (2015) and Abdulwhab and Kadhim (2018)), artificial intelligence (AI) (Qadir et al. (2015) and Roopaei et al. (2017)), and multimedia processing related technologies (Hu et al. (2018), Jadon (2018), and Ouddane and Faraoun (2018)). If the processing speed for such systems is not fast enough, however, it will cause recognition failure. Therefore, accelerating the image dehazing speed could significantly improve these systems.

The rest of this paper is organized as follows. In Section 2, the considered physical model for image dehazing is introduced. The proposed method is presented in Section 3. Section 4 presents the experimental results and discussion. Section 5 provides the study conclusions.

2 IMAGE DEHAZING PHYSICAL MODEL

THE widely used physical model for image dehazing, which was built based on light transmission in the air, is defined as follows (He et al. (2011))

$$\mathbf{I}(\mathbf{x}) = \mathbf{J}(\mathbf{x})t(\mathbf{x}) + \mathbf{A}(1 - t(\mathbf{x})), \quad (1)$$

where $\mathbf{x}$ is the pixel location, $\mathbf{I}$ is the intensity of the input hazy image, $\mathbf{J}$ is the scene radiance, which is the clear image without degrading, t is the image transmission, which expresses the part that can be captured by camera during light transmission, and $\mathbf{A}$ is the atmospheric light in a scene. In addition, in (1), $\mathbf{J}(\mathbf{x})t(\mathbf{x})$ describes the direct attenuation of the scene radiance within the media, where the reason for the attenuation is that when a light beam passes through air at the scene point, the light beam is scattered due to Rayleigh scattering and the extinction of light occurs due to interruption by the molecules of the particles in the air (McCartney (1976)). $\mathbf{A}(1\text{-}t(\mathbf{x}))$ describes the air-light being separated by the atmospheric light; the air-light refers to how when we look at a broad scene, there will be a bright scene point that gradually moves our focus to the horizon from the front view (Koschmieder (1924)).

Image blur occurs because the light emitted from the observed object is absorbed or scattered by the media in the air before it reaches the camera. When the atmosphere is homogeneous, the transmission $t(\mathbf{x})$ can be expressed as follows

$$t(\mathbf{x}) = e^{-\beta d(\mathbf{x})}, \quad (2)$$

where β is the scattering coefficient of the atmosphere and d is the scene depth, that is, the distance between the camera and the observed object. This equation indicates that the scene radiance is attenuated exponentially with the depth.

3 PROPOSED ALGORITHM

FIGURE 1 is a flowchart for the proposed image dehazing algorithm. The operation flow can be divided into the nine steps as follows:

Step 1: First, it is selected a haze image as input. In this case, an image with haze essentially means a blurred image.

Step 2: The image is then processed applying the White-Patch Retinex algorithm, and a new input with hazy image will be obtained to facilitate the subsequent operation.

Step 3: With this new input, a dark channel calculation is made based on the dark channel prior algorithm.

Step 4: After the dark channel is calculated, the top 0.1% of the pixels in terms of the pixel value are selected, and their pixel values in their corresponding positions in the original input image are obtained, after which the maximum value is designated as the atmospheric light.

Step 5: The obtained dark channel and atmospheric light are then combined to estimate the transmission map.

Step 6: Next, the transmission map is further enhanced by the median filter to reduce the creation of any halo effect.

Step 7: A guided image filter is subsequently used to smooth the edge of the transmission map and speed up the dehazing operation speed.

Step 8: The transmission map and atmospheric light obtained above are used to remove the image haze and make the image clear.

Step 9: Finally, we obtain a clear image output.

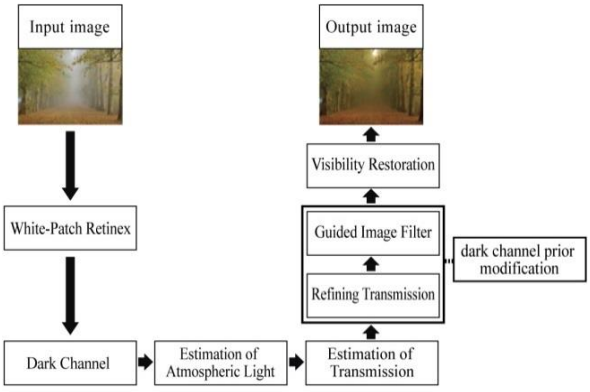

Figure 1. Flowchart of our proposed algorithm. (The originally input is from https://stackoverflow.com/questions/46315174/compare-the-difference-of-image-dehaze-algorithm-between-fotojet-and-polarr)

This flowchart shows that the study utilizes the algorithm proposed by He et al. (2011) and has added modules to develop a new algorithm and further improve performance. The additional components

include the White-Patch Retinex algorithm, the median filter (for refining transmission), and the guided image filter. It should be noted that the two boxes representing the refining transmission and guided image filter are the components that modified and improved the dark channel prior algorithm. Correspondingly, the visibility restoration operation also received effective adjustments. These added segments are cleverly and effectively placed and incorporated into the appropriate section of the flow process, such that their functions can be effectively utilized. In this manner, the issues faced by the He et al. algorithm are addressed effectively, allowing for better image dehazing performance. The following section provides a description of each segment.

3.1 White-Patch Retinex Algorithm

The surface of an object is reflected in different colors due to different lighting conditions. Humans are inherently capable of judging the true color of an object itself with enough surrounding information (Fairchild (2005)). We call the ability to judge the correct color of an object under different light conditions color constancy (Zeki (1993)). In contrast with humans, machines are not born with this ability. So, we hope that after being provided with an effective algorithm, machines will also possess this capability.

The purpose of color constancy is to restore an image to its original colors; it thus requires estimation of the light source intensity in the image. An image can be expressed using the following equation (Cepeda-Negrete (2012)):

$$f_c(x,y) = G(x,y)R_c(x,y)I_c, \tag{3}$$

where $f_c(x,y)$ is the pixel value of the pixel at position (x,y), $G(x,y)$ is the scene geometry factor of the image, $R_c(x,y)$ is the reflective coefficient of the pixel at position (x,y), and I_c is the image illumination. In general, the light source of color constancy has a uniform illumination; we thus assume $G(x,y) = 1$ and $R_c(x,y) = 1$, such that (3) is simplified to

$$f_c(x,y) = I_c. \tag{4}$$

The White-Patch Retinex algorithm can be used on color distortion images to restore their color constancy (Agarwal et al. (2006)). "Retinex" is an amalgamation of the Latin words Retina and Cortic, which refer to the retinal and cerebral scalp layers, respectively.

The simplified White-Patch Retinex algorithm states that the brightest pixel value of an RGB tri-channel is treated as the white of that channel; the other pixels are corrected in response. Denote $o_c(x,y)$ as the corrected pixel at (x,y), expressed as

$$o_c(x,y) = \frac{f_c(x,y)}{I_{c_{max}}}, \tag{5}$$

where

$$I_{c_{max}} = \max\{f_c(x,y)\}. \tag{6}$$

The simplified White-Patch Retinex algorithm can be improved to be more robust. To do so, determine the histogram of each of the color channels in the image, and then, instead of using the maximum pixel value as the reference point, set a specific percentage such that the cumulative pixel values are greater than a selected percentage of the total pixel amount as the reference point. This method has been used to remove shadow (Finlayson et al. (2006)). Let $f_c(j_c)$ denote the intensity of color channel c represented by bin j_c of the histogram H_c. Replace the denominator $I_{c_{max}}$ in (5) by $f_c(j_c)$, and then the output image pixels become

$$o_c(x,y) = \frac{f_c(x,y)}{f_c(j_c)}. \tag{7}$$

j_c shall satisfy the following two equations:

$$\gamma \le \sum_{k=j_c}^{n_b} H_c(k) \tag{8}$$

and

$$\gamma \ge \sum_{k=j_c+1}^{n_b} H_c(k). \tag{9}$$

In (8)-(9), n_b is the sum of bins in histogram $H_c(k)$ and γ is the selected percentage (normally about 1%) (Ebner (2007)). Note that, in our proposed algorithm, all pixel intensities in an input hazy image are scaled by using (7).

Figures 2(b) and 2(e) show the results of using the simplified White-Patch Retinex algorithm, whereas Figures 2(c) and 2(f) show the results of using the robust White-Patch Retinex algorithm. By comparing the 4 figures, we find that the results for the robust one are much better than those for the simplified one. Under different lights, this method can restore an object's original colors.

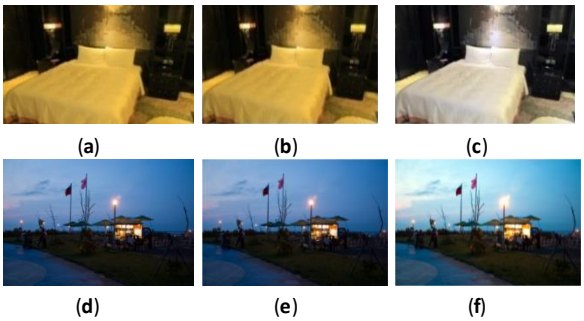

(a) (b) (c)

(d) (e) (f)

Figure 2. (a) **Image under yellow light,** (d) **image under ordinary outdoor light,** (b) **and** (e) **images after using the simplified White-Patch Retinex algorithm, and** (c) **and** (f) **images after using the robust White-Patch Retinex algorithm. (The originally inputs for** (a) **and** (d) **are from https://zi.media/@taiwantravelmap/post/HU3rEH and https://acswoa.tian.yam.com/posts/28989619, respectively)**

Images with dusty air normally will have serious color distortion problems because specific colors will be absorbed by particles in the air. Since the He et al. algorithm applies the same method to every channel, the restored image will still be plagued by color distortion problems. Therefore, we apply the White-Patch Retinex method to address the image haze issue and eliminate the color distortion problem.

Figure 3 is the result and color histogram of a street scene image with sandy haze that was treated using the improved White-Patch Retinex algorithm. It can be seen that the RGB distributions are different before the use of the White-Patch Retinex algorithm, but after using the White-Patch Retinex algorithm, the color channel distributions of the histogram are more similar. In this way, the color distortion will be reduced after we use the restoration equation.

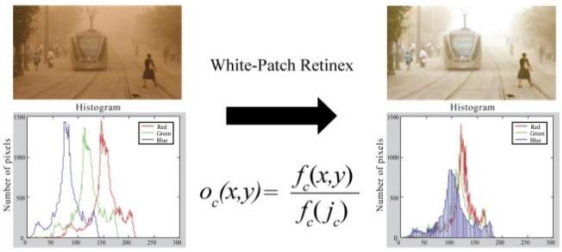

(a) (b)

Figure 3. (a) **Original image with haze and sandy scene and its color histogram, and** (b) **image and its color histogram after using the robust White-Patch Retinex algorithm. (The originally input is from https://aabgu.org/unseasonal-dust-storm-attributed-to-war-in-syria)**

3.2 Dark Channel

The dark channel prior algorithm is based on the observation that, in outdoor images that do not show the sky, the RGB values of the pixels will be presented such that the pixel value for at least one color will be very small and close to zero. The dark channel for an image **J** can be given by

$$J^{\text{dark}}(\mathbf{x}) = \min_{\mathbf{y}\in\Omega(\mathbf{x})}\left(\min_{c\in\{\text{r,g,b}\}} J^c(\mathbf{y})\right), \tag{10}$$

where J^c is a color channel of **J**, c is any channel of RGB, $\min_{c\in\{\text{r,g,b}\}}$ is the minimum value of the color channel at each pixel, $\Omega(\mathbf{x})$ is the **x**-centered patch, and $\min_{\mathbf{y}\in\Omega(\mathbf{x})}$ is a minimum filter used in $\Omega(\mathbf{x})$. He et al. analyzed the results of many images and reported that in no-sky outdoor images, the **J** dark channel intensity is very small and mostly approaches zero. They thus made the following assumption

$$J^{\text{dark}}(\mathbf{x}) \to 0. \tag{11}$$

This observation is called the dark channel prior.

Figure 4 presents an image obtained through dark channel calculation, where Figure 4(a) is a no-sky image. After passing through the first minimum operator, taking the minimum value of the color channel at each pixel, we obtain Figure 4(b); after using the minimum filter in $\Omega(\mathbf{x})$, we then obtain Figure 4(c).

(a) (b) (c)

Figure 4. Dark channel calculation: (a) **input image,** (b) **determining the minimum value of RGB at each pixel, and** (c) **using a 15x15 window to apply a minimum filter to** (b)**. (The originally input is from https://abc.2008php.com/tu_shouji.php?id=902568&topy=11)**

3.3 Estimation of Atmospheric Light

Figure 5 shows that the dark channel of a hazy image approximates the haze density. The darker the pixel is, the less the haze is, and vice versa. Therefore, the dark channel can be used to detect the most haze-opaque region and improve the atmospheric light estimation. He et al. selected the 0.1% of the pixels with the highest luminous intensity and recorded their positions. The corresponding intensity levels for these positions in the original foggy input image were then obtained. From this intensity data, the maximum value was then designated as atmospheric light.

(a) (b)

Figure 5. (a) **Hazy image, and** (b) **dark channel of** (a)**. (The originally input is from http://dinosauriens.info/?u=Air++Minnesota+Pollution+Control+Agency)**

3.4 Estimation of Transmission Map

First, (1) is normalized by the atmospheric light **A**:

$$\frac{I^c(\mathbf{x})}{A^c} = t(\mathbf{x})\frac{J^c(\mathbf{x})}{A^c} + 1 - t(\mathbf{x}),\ c \in \{\mathrm{r},\ \mathrm{g},\ \mathrm{b}\}. \quad (12)$$

Assume that the transmission in a local patch is constant, expressed by $\tilde{t}(\mathbf{x})$. Next, using the dark channel calculation on both sides of the equal mark (=) in (12), we have

$$\min_{\mathbf{y}\in\Omega(\mathbf{x})}\left(\min_{c\in\{\mathrm{r,g,b}\}}\frac{I^c(\mathbf{y})}{A^c}\right) = \tilde{t}(\mathbf{x})\min_{\mathbf{y}\in\Omega(\mathbf{x})}\left(\min_{c\in\{\mathrm{r,g,b}\}}\frac{J^c(\mathbf{y})}{A^c}\right) + 1 - \tilde{t}(\mathbf{x}). \quad (13)$$

From the dark channel prior, we can then obtain

$$\min_{\mathbf{y}\in\Omega(\mathbf{x})}\left(\min_{c\in\{\mathrm{r,g,b}\}}\frac{J^c(\mathbf{y})}{A^c}\right) = 0. \quad (14)$$

From (13)-(14), we can obtain the transmission as

$$\tilde{t}(\mathbf{x}) = 1 - \min_{\mathbf{y}\in\Omega(\mathbf{x})}\left(\min_{c\in\{\mathrm{r,g,b}\}}\frac{I^c(\mathbf{y})}{A^c}\right). \quad (15)$$

However, in practice, the atmosphere, even on clear days, contains a small amount of particulate. Therefore, if the haze is completely removed, the scene looks unnatural. Haze is a factor that helps people to sense the depth of an image, so it is better to keep a very small amount in an image by introducing a constant parameter α, where $0 < \alpha \le 1$, which makes the image seem more natural. The transmission map can then be rewritten as follows

$$\tilde{t}(\mathbf{x}) = 1 - \alpha \min_{\mathbf{y}\in\Omega(\mathbf{x})}\left(\min_{c\in\{\mathrm{r,g,b}\}}\frac{I^c(\mathbf{y})}{A^c}\right). \quad (16)$$

3.5 Refining Transmission

The transmission reinforcement is based on the improvement of the dark channel prior algorithm. For the dark channel prior algorithm to perform a transmission calculation, it needs to use a minimum filter; however, a minimum filter will cause edge data loss in window selection, forming a halo due to depth discontinuities. Thus, Gibson et al. (2010) and Huang et al. (2014) suggested using a median filter to retain the edge data of hazy images and avoid the halo effect.

Figure 6(a) is a grayscale image of a hazy image input, and the pixel value of the red frame is 127. Figure 6(b) is the grayscale image after a minimum filter is used, and the pixel value of the red frame is 45; Figure 6(c) is the grayscale image after using a median filter, and the pixel value of the red frame is 156. By comparing Figures 6(b) and 6(c), it can be seen that the edges are different under different filters, and the median filter can retain edges more effectively than the minimum filter. The pixel value of the red frame indicates that the pixel quality of the image after applying the median filter is close to the grayscale image of the original input image, while the image error using the minimum filter is larger.

(a) (b) (c)

Figure 6. Comparison of using the median filter and the minimum filter: (a) grayscale image of hazy image input, (b) grayscale image after using the minimum filter, and (c) grayscale image after using the median filter. (The originally input is from https://www.groundai.com/project/dr-net-transmission-steered-single-image-dehazing-network-with-weakly-supervised-refinement)

Next, we use the method proposed by Huang et al. (2014) to detect the edge information $D(\mathbf{x})$:

$$D(\mathbf{x}) = \alpha(\min(\underset{\mathbf{y}\in\Omega(\mathbf{x})}{\mathrm{median}}(W(\mathbf{y})), W(\mathbf{x}))) - \min_{\mathbf{y}\in\Omega(\mathbf{x})} W(\mathbf{y}), \quad (17)$$

where α is set to 0.95, $\underset{\mathbf{y}\in\Omega(\mathbf{x})}{\mathrm{median}}$ is a median filter, $\min_{\mathbf{y}\in\Omega(\mathbf{x})}$ is a minimum filter, and W is the minimum value of the color channels in the input hazy image. The refined transmission is defined as $t_r(\mathbf{x})$, which is given by

$$t_r(\mathbf{x}) = \tilde{t}(\mathbf{x}) - D(\mathbf{x}), \quad (18)$$

where $\tilde{t}(\mathbf{x})$ is the transmission map after calculating (16). Figure 7 shows a concept procedure for refining the transmission.

3.6 Guided Image Filter

In order to solve the time complexity of soft matting used in image dehazing specified in the algorithm of He et al., many scholars have proposed using different methods, such as using a bilateral filter (Sun et al. (2010), Furukawa et al. (2014), and Sun et al. (2011)). However, the computational complexity of a bilateral filter is very large, and image distortion occurs in some cases with gradient reversal. He et al. (2013) subsequently proposed the guided image filter. Since it utilizes the linear combination method to perform the calculations, requires no complex mathematical operations, and allows for the output image to have the same gradient direction as the guidance image, this method gradually came to be used for haze removal. Choosing a guided image filter not only increases the operation speed but also makes the transmission map smoother and retains its edge and gradient.

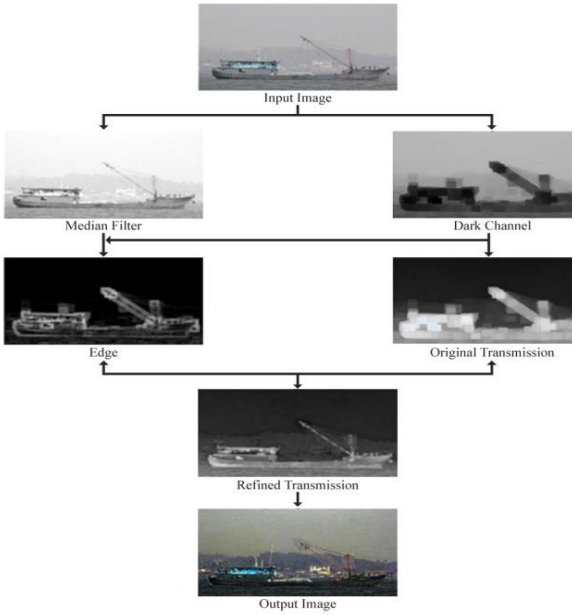

Figure 7. Procedure for refining the transmission map. (The originally input is from https://www.gettyimages.fr/%C3%A9v%C3%A9nement/haze-blankets-indonesia-as-fires-worsen-171135432#/motorists-pass-through-haze-pollution-on-june-20-2013-in-bintan-the-picture-id170904195)

Define q_i as the ith output pixel, p_i as the ith input pixel, n_i as the ith input pixel noise component, I_i is the ith pixel of the guidance image, and ω_k is the window with the kth pixel as the center. The presence of a local linear model between I_i and q_i constitutes the key assumption of the guided image filter. That is, an assumption that q_i consists of a linear transform of I_i within a window ω_k centered at the pixel k is made, yielding the following (He et al. (2013)):

$$q_i = a_k I_i + b_k, \ \forall i \in \omega_k , \tag{19}$$

where it is assumed that a_k and b_k are coefficients that are constant in ω_k. In (19), q_i is calculated as n_i subtracted from p_i:

$$q_i = p_i - n_i . \tag{20}$$

From (19) and (20), we can get

$$n_i = a_k I_i + b_k - p_i . \tag{21}$$

Then, the cost function $E(a_k, b_k)$ in the window ω_k is minimized as follows

$$\min E(a_k, b_k) = \min \sum_{i \in \omega_k} (n_i^2 + \varepsilon a_k^2) , \tag{22}$$

where ε is a parameter used to keep a_k from becoming too big.

Via (19)-(22), we can find a_k and b_k:

$$a_k = \frac{\frac{1}{|\omega|}\sum_{i \in \omega_k} I_i p_i - \mu_k \bar{p}_k}{\sigma_k^2 + \varepsilon} \tag{23}$$

and

$$b_k = \bar{p}_k - a_k \mu_k , \tag{24}$$

where μ_k and σ_k^2 are mean and variance values in ω_k, $|\omega|$ is the sum of pixels in ω_k, and $\bar{p}_k = \frac{1}{|\omega|}\sum_{i \in \omega_k} p_i$ is the mean value of pixels in ω_k.

Since pixel i may be included not merely in the single window ω_k, q_i in (19) will vary in a different window ω_k. After calculating all a_k and b_k values in ω_k, the following equation is used to obtain the final q_i:

$$q_i = \frac{1}{|\omega|}\sum_{k: i \in \omega_k} (a_k I_i + b_k) . \tag{25}$$

From Figure 8, we can see the dehazing effect of the guided image filter.

(a) (b) (c)

Figure 8. Guided image filter: (a) input image, (b) guidance image, and (c) output image. (The originally input is from https://pixabay.com/zh)

3.7 Visibility Restoration

By the transmission and atmospheric light obtained above, we can restore an image via the following equation:

$$J^c(\mathbf{x}) = \frac{I^c_{\text{new}} - A^c}{\max(t(\mathbf{x}), t_0)} + A^c, \ c \in \{\text{r,g,b}\} , \tag{26}$$

where I^c_{new} is the new input image with haze after the White-Patch Retinex algorithm was used and $t(\mathbf{x})$ is the enhanced transmission map after being processed through the guided image filter.

4 RESULTS AND DISCUSSION

THIS section presents the full-range experimental results and discusses our proposed algorithm. We used Matlab R2014 and a 2.7GHz Intel quad-core processor-based desktop computer to run this algorithm. For the experimental test, the setting values found in He et al. (2011), He et al. (2013), and Ebner, M. (2007) served as the primary references for determining the parameter setting values used in the equations described in Section 3. The blurry and foggy image data used in this experiment were mainly obtained through web searches (the source URLs of

these images are indicated in their respective figure captions).

Recall that the three problems that the dark channel prior algorithm brings are that: it will create the halo effect, it will cause color distortion, and it takes a long time to restore the image. Given the above concerns, we provide a complete comparison of our algorithm with the algorithm of He et al. (2011). Specifically, we examine the results of image restoration using a combination of the White-Patch Retinex algorithm and the improved dark channel prior algorithm, particularly with regard to the image restoration effort and its effectiveness and applicability against these three problems. In addition, we also perform an image quality assessment to numerically demonstrate our algorithm's advantages.

4.1 Halo Effect

This section discusses whether the halo effect can be effectively eliminated by our proposed algorithm. Three types of scenes are distinguished from the degree of contact with the sky, arranged in descending order by size, they are the village scene image, city building image and forest scene image, as shown in Figures 9(a), 10(a), and 11(a), respectively. The sky is a place that represents space without boundaries, so the likelihood that discontinuity will occur will be greatly increased. If the part in contact with the sky is larger, the halo effect will be stronger. This phenomenon can be seen from the placement of the red frame in Figures 9(b), 10(b), and 11(b). Note that, in Figure 11(b), there is no halo effect between the leaves and the sky; it is believed that this occurred as the sky illumination of the originally input image is very high, to the extent that the level of illumination was similar to that of the halo, thus the halo is integrated into the bright portion and becomes unobservable. However, for the trees in the lower part of the figure, it can be seen that the gap between the front and back trees still caused a halo effect. However, the images generated by our proposed algorithm show almost no halo effect. Because we use the median filter to preserve the edge, even if the minimum filter is still used, the median filter (in the previous layer) would still effectively retain the image edge at the place that contacts the distant sky. By observing Figures 9(d), 10(d), and 11(d), we can see that the transmission image using the He et al. algorithm shows an apparently blurry view at the junction with the sky. In addition, the boundaries of the objects are not as clear as they are in the image created by using the algorithm we have proposed.

In fact, through the observation of the transmission map, we can determine whether the resulting image will inevitably produce the halo effect. From Figures 9(d), 10(d), and 11(d), we have already found that the transmission has already produced halo at the discontinuity; therefore, restoring the image will generate halo. As we can see from Figures 9(c), 10(c), and 11(c), our proposed algorithm can effectively solve the problem of the halo effect.

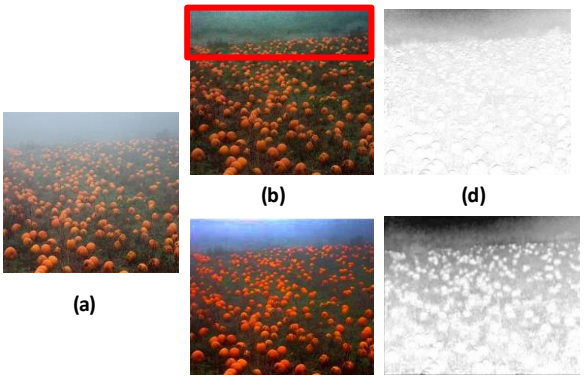

Figure 9. Village scene image: (a) originally input, (b) modified by the He et al. algorithm, (c) modified by the new algorithm we have proposed, (d) transmission of (b), and (e) transmission of (c). (The originally input is from the aforementioned study by Zhu et al. (2015))

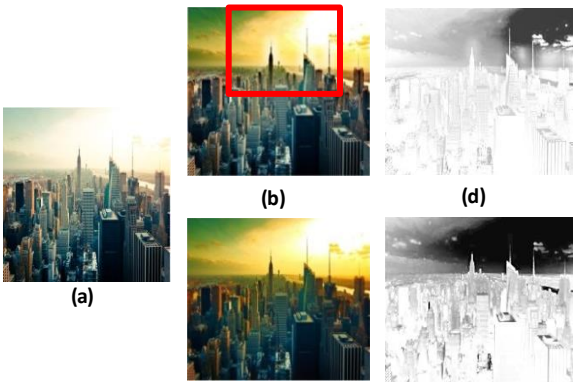

Figure 10. City building image: (a) originally input, (b) modified by the He et al. algorithm, (c) modified by the new algorithm we have proposed, (d) transmission of (b), and (e) transmission of (c). (The originally input is from http://www.unizyx.com.tw/governance.php)

4.2 Color Distortion

In this section, we discuss the capability of the new algorithm we have proposed to reduce color distortion. Two categories are established: one for input images that have no color distortion, and the other one for input images with color distortion.

Figure 12(a) and Figure 13(a) belong to category 1. From them, we can see that the histograms distribute similarly on each color channel. For Figure 12(a), after being processed by the He et al. algorithm and the new algorithm we have proposed, at the low-illumination portion, the first half of color histogram keeps the similar distribution, whereas for the other half (at the high-illumination portion), its proportions of red and green lights are less and its blue light remains unchanged because that sky is blue. After the

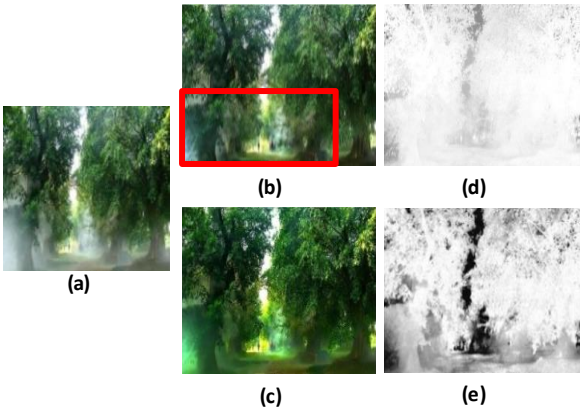

Figure 11. Forest scene image: (a) originally input, (b) modified by the He et al. algorithm, (c) modified by the new algorithm we have proposed, (d) transmission of (b), and (e) transmission of (c). (The originally input is from http://blog.sina.com.cn/s/blog_4a8715500102v845.html)

aforesaid two algorithms are applied to Figure 13(a), the colors distribute similarly; however, the halo effect still exists when using the He et al. algorithm and it can be seen around the motorcycle (as shown in Figure 13(b)).

Figure 14(a) and Figure 15(a) belong to category 2. Since the medium in the air absorbs specific colors in the light, the color histogram will show an inconsistent distribution. Therefore, we hope to restore the color constancy of the image through the White-Patch Retinex algorithm so that its color histogram can be consistently distributed. From Figures 14(c) and 15(c), it can be seen that using the He et al. algorithm, color distortion still exists after dehazing, such that the entire image is still yellow and the color histogram is still not consistently distributed. Because this algorithm assumes that each color channel uses the same recovery equation, it does not take the fact that the light-absorption degrees of different particles are not the same into account. Figures 14(b) and 15(b) are new image inputs after being processed by the White-Patch Retinex algorithm. It can be seen from the respective color histograms that their distributions are similar to the original one. With these new image inputs, we performed image dehazing once again. Figures 14(d) and 15(d) are the corresponding resulting images. It can be seen that the degree of color distortion has been greatly reduced, such that we can clearly see the blue locomotive in Figure 14(d) and the illuminated sky at the back of Figure 15(d).

4.3 *Image Quality Testing*

Image quality testing can generally be categorized into two types, that is, tests with reference standards and tests without reference standards. Since there are no clear definitions or standard rules for determining what a clear image is, this study went with the "no reference standards" approach. The image quality assessment that was performed in this study utilized a method that involves the quality quantification of images and visual scoring that is consistent with human subjectivity (Hautiere et al. (2008)). Three parameters, namely, e, $\bar{r}$, and σ, are defined for this method and described below:

(a) e is the ratio of the newly added edges and indicates whether the method in question is able to restore the edges that are not visible in the original image, and it may be expressed as

$$e = \frac{n_r - n_o}{n_o}, \tag{27}$$

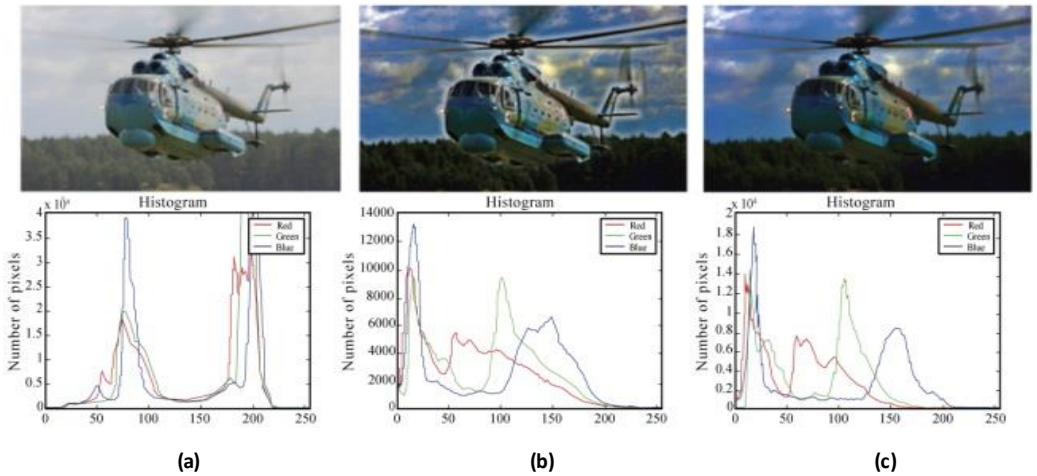

Figure 12. Helicopter image and its color histogram: (a) originally input, (b) modified by the He et al. algorithm, and (c) modified by the new algorithm we have proposed. (The originally input is from https://pl.wikipedia.org/wiki/Plik:Mi-14_0083.JPG)

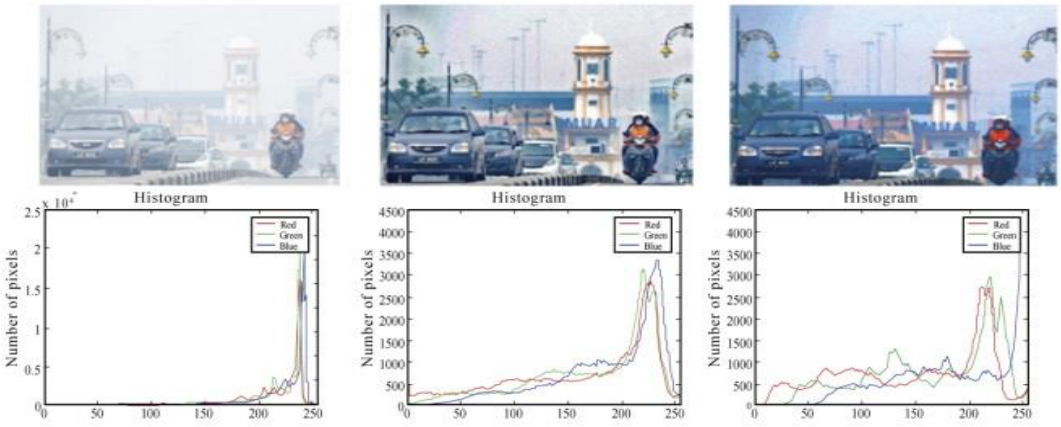

Figure 13. Street image and its color histogram: (a) originally input, (b) modified by the He et al. algorithm, and (c) modified by the new algorithm we have proposed. (The originally input is from http://ca.ntdtv.com/xtr/gb/2013/06/23/a919271.html)

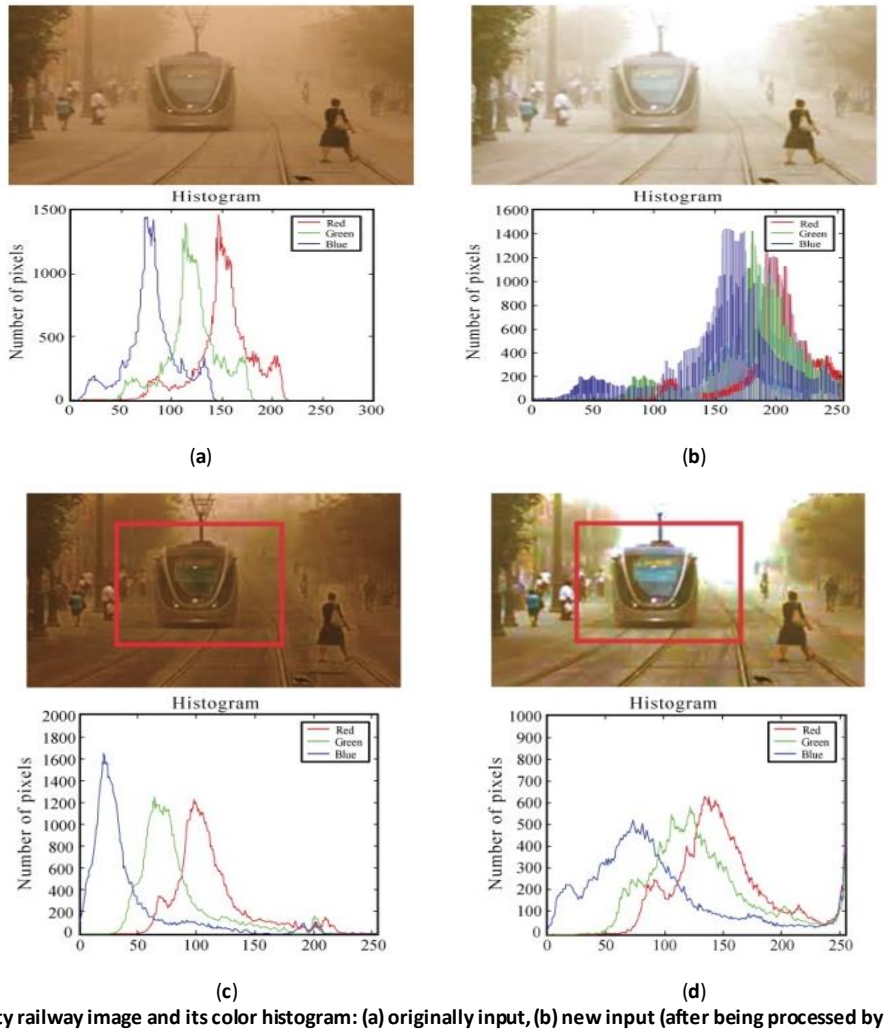

Figure 14. Dusty railway image and its color histogram: (a) originally input, (b) new input (after being processed by the White-Patch Retinex algorithm), (c) modified by the He et al. algorithm, and (d) modified by the new algorithm we have proposed. (The originally input is from https://aabgu.org/unseasonal-dust-storm-attributed-to-war-in-syria)

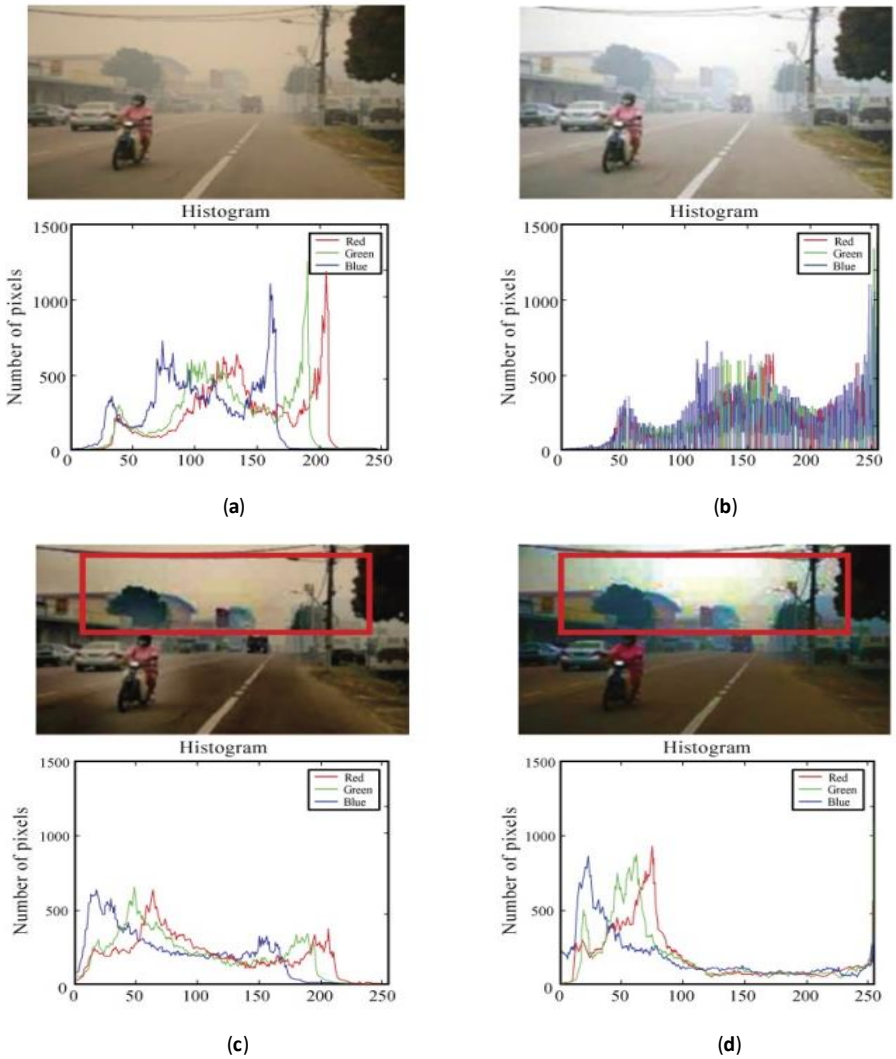

Figure 15. Dusty street image and its color histogram: (a) originally input, (b) new input (after being processed by the White-Patch Retinex algorithm), (c) modified by the He et al. algorithm, and (d) modified by the new algorithm we have proposed. (The originally input is from http://recap.asia/climate-journal/malaysia-must-own-up-to-its-hand-in-haze-menace)

where n_r and n_o are the number of edges visible in the restored image and foggy image, respectively.

(b) $\bar{r}$ is the visible edge gradient ratio of the foggy and restored images (in contrast to (27), the edges in the foggy image that are visible or not visible are considered), and it may be expressed as

$$\bar{r} = \exp\left[\frac{1}{n_r}\sum_{P_i \in R} \log r_i\right], \tag{28}$$

where R is the set of visible edges in the restored image, P_i is the cardinal number of the visible edges in R, and r is defined as

$$r = \frac{L_r}{L_o}, \tag{29}$$

where L_r is the visibility level of the restored image and L_o is the visibility level of the foggy image.

(c) σ represents the oversaturation level of the restored image and may be expressed as

$$\sigma = \frac{n_s}{\dim_x \times \dim_y}, \tag{30}$$

where n_s is the total number of pixels that are not oversaturated in the original image but are oversaturated in the defogged image and $\dim_x \times \dim_y$ are the dimensions of the image.

Ideally, the quality is better when e and $\bar{r}$ are higher and σ is smaller. Using Figures 9-15 to obtain the results numerically, as shown in Table 1, it is clear that the new algorithm that we have proposed was able to produce a good restorative effect for images with

different scenes. The e and $\bar{r}$ values showed that the new algorithm we have proposed was better at preserving the edges compared to the He et al. algorithm. This was achieved by enhancing the transmission at the edges, such that the edges that were originally not identifiable in the foggy image can now be identified. As for the σ values, they indicated that the new algorithm we have proposed was able to preserve the image's colors after restoring the image and did not cause oversaturation or darken the image excessively.

Table 1. Comparison of e, $\bar{r}$, and σ using the He et al. algorithm and the new algorithm we have proposed for dehazing different images; the before and after "/" values represent the test results for the He et al. algorithm and the new algorithm we have proposed, respectively.

Item / Figure no.	e	$\bar{r}$	σ
Figure 9	-0.1543 / -0.0902	1.0050 / 1.0050	0.0116 / 0
Figure 10	-0.1314 / -0.0720	1.0010 / 1.0090	0 / 0
Figure 11	-0.1412 / -0.0897	1.0060 / 1.0090	0 / 0
Figure 12	-0.0717 / -0.0127	1.0007 / 1.0007	0.0143 / 0.0129
Figure 13	-0.0828 / -0.0329	1.0007 / 1.0007	0 / 0
Figure 14	-0.1898 / -0.1531	1.0020 / 1.0065	0.0029 / 0.0001
Figure 15	-0.1935 / -0.1650	1.0031 / 1.0082	0.0269 / 0.0115

4.4 Time Spent

Last, we explore whether or not the new algorithm we have proposed can increase the processing speed. There are 7 hazy images arranged in order of their image size. The images are presented in Figures 16 to 22, from small to large. Table 2 lists the dehazing time spent on the different sized images by the He et al. algorithm and the one we have proposed, respectively. It is found that, no matter what algorithm is applied, the bigger images require more processing time; however, in terms of the rate at which the processing time required increases in relation to image size, this rate is significantly higher for the He et al. algorithm when compared to the algorithm we have proposed. The main reason is because the soft matting applied in the He et al. algorithm requires the use of the Laplacian matrix, which requires massive and complex mathematic calculations for each single pixel; yet, the guided image filter itself does not use complex mathematic calculations and is a linear filter, thus the processing time spent is far shorter than that of the soft matting.

(a) (b) (c)

Figure 16. (a) 276 x 183 hazy image, (b) modified by the He et al. algorithm, and (c) modified by the new algorithm we have proposed. (The originally input is from http://www.ifanr.com/app/680110)

(a) (b) (c)

Figure 17. (a) 512 x 341 hazy image, (b) modified by the He et al. algorithm, and (c) modified by the new algorithm we have proposed. (The originally input is from https://phys.org/news/2016-12-planes-grounded-smog-china-day.html)

(a) (b) (c)

Figure 18. (a) 612 x 612 hazy image, (b) modified by the He et al. algorithm, and (c) modified by the new algorithm we have proposed. (The originally input is from https://commons.wikimedia.org/wiki/File:The_flashpoint_of_the_Wushe_Incident.jpg)

(a) (b) (c)

Figure 19. (a) 780 x 520 hazy image, (b) modified by the He et al. algorithm, and (c) modified by the new algorithm we have proposed. (The originally input is from https://www.straitstimes.com/singapore/environment/hazy-skies-in-singapore-on-wednesday-morning-as-psi-hovers-in-moderate-range)

(a) (b) (c)

Figure 20. (a) 1208 x 745 hazy image, (b) modified by the He et al. algorithm, and (c) modified by the new algorithm we have proposed. (The originally input is from http://blog.sina.com.cn/s/blog_4a8715500102v845.html)

(a) (b) (c)

Figure 21. (a) 1272 x 959 hazy image, (b) modified by the He et al. algorithm, and (c) modified by the new algorithm we have proposed. (The originally input is from https://www.linkedin.com/pulse/winonas-womb-hilary-flanery-long-skirts-tc)

(a) (b) (c)

Figure 22. (a) 2592 x 3872 hazy image, (b) modified by the He et al. algorithm, and (c) modified by the new algorithm we have proposed. (The originally input is from https://commons.wikimedia.org/wiki/File:Germany-Farchant-Landscape.JPG)

Table 2. Comparison of processing time using the He et al. algorithm and the new algorithm we have proposed for the dehazing of different sized images.

Item / Figure no.	Image size	Time spent using the He et al. algorithm	Time spent using the new algorithm we have proposed
Figure 16	276 x 183	4.9709 sec	0.6409 sec
Figure 17	512 x 341	34.3165 sec	2.2248 sec
Figure 18	612 x 612	50.2648 sec	4.8361 sec
Figure 19	780 x 520	90.6524 sec	5.1769 sec
Figure 20	1208 x 745	above 2 min	11.9691 sec
Figure 21	1272 x 959	above 4 min	16.5952 sec
Figure 22	2592 x 3872	above 30 min	151.7793 sec

5 CONCLUSIONS

IN this paper, we have successfully combined two heterogeneous algorithms, namely, the White-Patch Retinex algorithm and a modified dark channel prior algorithm, to create a new algorithm for dehazing single images, thus solving the problems that occur with existing single image dehazing systems (i.e., the halo effect, color distortion, and excessive processing time). We combine the dark channel and median filter to find a suitable edge, address the halo effect and artificial boundary created at the discontinuous boundary particularly at spots where the distance between the sky and objects is extremely large. Reducing the halo effect can make the overall image seem more natural and harmonious. Meanwhile, using the guided image filter to replace the soft matting makes the edge of a transmission map smoother and increases the dehazing process speed. In addition, we use the White-Patch Retinex algorithm to determine specific pixel values through the histogram, make corrections to the entire image, restore the color-distorted image, and maintain the image color at a constancy that is closer to the human visual mode. The full-range experimental results showed that, in terms of the halo effect, color distortion, and time spent, the new image dehazing algorithm we have proposed is superior to the conventional algorithm. Furthermore, an image quality assessment was performed to test the new algorithm that we have proposed, and the results showed that the image boundary recovery and color saturation were good. With improvements to computing power, the use of our proposed algorithm in real-time applications will become feasible in the future when it is paired with computers with better computing performance. Therefore, based on the aforesaid observations and reasons, we believe that the new algorithm that we have proposed can serve as a good image dehazing candidate to be applied to various sensing systems and emerging technological systems such as self-driving vehicles and drones. At the same time, self-driving vehicles and drones will become the primary application platforms that emerging technologies such as 5G and AI as well as multimedia processing related technologies will be utilized in. Therefore, it is recommended that future studies look into how our proposed image dehazing algorithm can be effectively integrated into technologies associated with 5G and AI as well as multimedia processing related technologies. In addition, future studies could also conduct comprehensive and fair comparisons of the algorithm's performance relative to other non-dark channel prior methods.

6 REFERENCES

Abdulwhab, W. and Kadhim, A. (2018). Comparative study of channel coding schemes for 5G, *Journal of Electronic Systems*, 8(3), 95–102.

Agarwal, V., Abidi, B.R., Koschan, A., and Abidi, M.A. (2006). An overview of color constancy algorithms. *J. Pattern Recognition Research*, 1(1), 42–54.

BBC News: Dust from northern China sweeps over Taiwan. (2010). Available online: https://www.bbc.com/zhongwen/trad/china/2010/03/100322_taiwan_sandstorm

Cepeda-Negrete, J. and Sanchez-Yanez, R.-E. (2012). Combining color constancy and gamma correction for image enhancement, *Proceedings of the IEEE Ninth Electronics, Robotics and Automotive Mechanics Conference*, Cuernavaca, Mexico.

Cho, Y., Shin, Y.-S., and Kim, A. (2016). Online depth estimation and application to underwater image dehazing, *Proceedings of the OCEANS 2016 MTS/IEEE Monterey*, Monterey, CA, USA.

Ebner, M. (2007). *Color Constancy*, 1st ed., J. Wiley and Sons, Eds. Wrzburg, Germany: Wiley Publishing.

El-Hashash, M.M., Aly, H.A., Mahmoud, T.A., and Swelam, W. (2015). A video haze removal system on heterogeneous cores, *Proceedings of the IEEE Global Conference on Signal and Information Processing*, Orlando, FL, USA.

Fairchild, M.D. (2005). *Color Appearance Models*, 2nd ed., Hoboken, NJ: John Wiley and Sons.

Fattal, R. (2008). Single image dehazing, *ACM Trans. Graphic.*, 27, article no. 72.

Finlayson, G.D., Hordley, S.D., Lu, C., and Drew, M.S. (2006). On the removal shadows from images. *IEEE Trans. Pattern Anal. Mach. Intell.*, 28(1), 59–68.

Furukawa, S., Fukuda, T., Koga, T., Suetake, N., and Uchino, E. (2014). High-speed min-max bilateral filter-based image dehazing by using GPGPU, *Proceedings of the International Conference on Advanced Mechatronic Systems*, Kumamoto, Japan.

Gibson, K., Vo, D., and Nguyen, T. (2010). An investigation in dehazing compressed images and video, *Proceedings of the OCEANS 2010 MTS/IEEE SEATTLE*, Seattle, WA, USA.

Gupta, A. and Jha, R.K. (2015). A survey of 5G network: Architecture and emerging technologies. *IEEE Access*, 3, 1206–1232.

Hautiere, N., Tarel, J.-P., and Aubert, D. (2007). Towards fog-free in-vehicle vision systems through contrast restoration, *Proceedings of the IEEE Conference on Computer Vision and Pattern Recognition, Minneapolis*, MN, USA.

Hautiere, N., Tarel, J.-P., Aubert, D., and Dumont, E. (2008). Blind contrast enhancement assessment by gradient ratioing at visible edges, *Image Analysis & Stereology Journal*, 27(2), 87–95.

He, K., Sun, J., and Tang, X. (2011). Single image haze removal using dark channel prior, *IEEE Trans. Pattern Anal. Mach. Intell.*, 33(12), 2341–2353.

He, K., Sun, J., and Tang, X. (2013). Guided image filtering, *IEEE Trans. Pattern Anal. Mach. Intell.*, 35(6), 1397–1409.

Hsieh, C.-H., Lin, Y.-S., and Chang, C.-H. (2014). Haze removal without transmission map refinement based on dual dark channels, *Proceedings of the International Conference on Machine Learning and Cybernetics*, Lanzhou, China.

Hsieh, C.-H., Chen, C.-Y., and Dai, Y.-J. (2016). Single image dehazing based on pixel minimum channel, *Proceedings of the IEEE Symposium Series on Computational Intelligence*, Athens, Greece.

Hu, C., Zhai, G., and Li, D. (2015). An Augmented-Reality night vision enhancement application for see-through glasses, *Proceedings of the IEEE International Conference on Multimedia & Expo Workshops*, Turin, Italy.

Hu, G., Rong, J., Kou, W., Yuenyong, S., and Qu, J. (2018). A noise-robust image encryption algorithm based on hyper chaotic cellular neural network, *Journal of Digital Information Management*, 16(5), 246–257.

Huang, S.-C., Chen, B.-H., and Wang, W.-J. (2014). Visibility restoration of single hazy images captured in real-world weather conditions, *IEEE Trans. Circuits Syst. Video Technol.*, 24(10), 1814–1824.

Jadon, M. (2018). A novel method for leaf area estimation based on Hough transform, *Journal of Multimedia Processing and Technologies*, 9(2), 33–44.

Ji, X., Cheng, J., Bai, J., Zhang, T., and Wang, M. (2014). Real-time enhancement of image clarity for traffic video monitoring system in haze. *Proceedings of the Seventh International Congress on Image and Signal Processing*, Dalian, China.

Kim, T.K., Paik, J.K., and Kang, B.S. (1998). Contrast enhancement system using spatially adaptive histogram equalization with temporal filtering, *IEEE Trans. Consum. Electr.*, 44(1), 82–87.

Kopt, J., Neubert, B., Chen, B., Cohen, M., Cohen-Or, D., Deussen, O., Uyttendaele, M., Lischinski, D. (2008). Deep photo: model-based photograph enhancement and viewing. *ACM Trans. Graphic.*, 27, article no. 116.

Koschmieder, H. (1924). Theorie der horizontalen sichtweite, *Beitr. Phys. Freien Atm.*, 12(33-53), 171–181.

Land, E.H. and McCann, J.J. (1971). Lightness and retinex theory, *J. Opt. Soc. Am.*, 61(1), 1–11.

Long, J., Shi, Z., and Tang, W. (2012). Fast haze removal for a single remote sensing image using dark channel prior, *Proceedings of the International Conference on Computer Vision in Remote Sensing*, Xiamen, China.

Lu, X., Lv, G., and Lei, T. (2014). Fast single image dehazing algorithm, *Proceedings of the International Conference on Audio, Language and Image Processing*, Shanghai, China.

Mai, J., Zhu, Q., Wu, D., Xie, Y., and Wang, L. (2014). Back propagation neural network dehazing, *Proceedings of the IEEE International Conference on Robotics and Biomimetics*, Bali, Indonesia.

McCartney, E.J. (1976). *Optics of the Atmosphere: Scattering by Molecules and Particles*, New York, John Wiley and Sons, Inc..

Meng, G., Wang, Y., Duan, J., Xiang, S., and Pan, C. (2013). Efficient image dehazing with boundary constraint and contextual regularization,

Proceedings of the IEEE International Conference on Computer Vision, Sydney, NSW, Australia.
Nair, D. and Sankaran, P. (2015). A modified dark channel prior for improved dehazing, *Proceedings of the IEEE Recent Advances in Intelligent Computational Systems*, Trivandrum, India.
Narasimhan, S.G. and Nayar, S.K. (2003). Contrast restoration of weather degraded images, *IEEE Trans. Pattern Anal. Mach. Intell.*, 25(6), 713–724.
Nayar, S.K. and Narashiman, S.G. (1999). Vision in bad weather, *Proceedings of the Seventh IEEE International Conference on Computer Vision*, Kerkyra, Greece.
Ouddane, S. and Faraoun, K. M. (2018). Asymmetric stereoscopic images coding using perceptual model, *Journal of Multimedia Processing and Technologies*, 9(2), 59–70.
Pan, X., Xie, F., Jiang, Z., and Yin, J. (2015). Haze removal for a single remote sensing image based on deformed haze imaging model, *IEEE Signal Process. Lett.*, 22(10), 1806–1810.
Qadir, J., Yau, K.-L. A., Imran, M.A., Ni, Q., and Vasilakos, A.V. (2015). Artificial intelligence enabled networking, *IEEE Access*, 3, 3079–3082.
Roopaei, M., Rad, R., and Jamshidi, M. (2017). Deep learning control for complex and large scale cloud systems, *Intell. Autom. Soft Comput*., 23(3), 389–391.
Saggu, M.K. and Singh, S. (2015). A review on various haze removal techniques for image processing, *Int. J. Current Engineering and Technology*, 5(3), 1500–1505.
Schechner, Y.Y., Narasimhan, S.G., and Nayar, S.K. (2001). Instant dehazing of images using polarization, *Proceedings of the IEEE Conference on Computer Vision and Pattern Recognition*, Kauai, HI, USA.
Shiau, Y.-H., Yang, H.-Y., Chen, P.-Y., and Chuang, Y.-Z. (2013). Hardware implementation of a fast and efficient haze removal method, *IEEE Trans. Circuits Syst. Video Technol.*, 23(8), 1369–1374.
Shwartz, S., Namer, E., and Schechner, Y.Y. (2006). Blind haze separation, *Proceedings of the IEEE Conference on Computer Vision and Pattern Recognition*, NY, USA.
Singh, D. and Kumar, V. (2018). Comprehensive survey on haze removal techniques, *Multimedia Tools and Applications*, 77(8), 9595–9620.
Stark, J.A. (2000). Adaptive image contrast enhancement using generalizations of histogram equalization, *IEEE Trans. Image Process.*, 9(5), 889–896.
Sun, K., Wang, B., Zheng, Z., and Zhou, Z. (2010). Fast single image dehazing using iterative bilateral filter, *Proceedings of the Second International Conference on Information Engineering and Computer Science*, Wuhan, China.
Sun, K., Wang, B., Zhou, Z.-Q., and Zheng, Z.-H. (2011). Real time image haze removal using bilateral filter, *Trans. Beijing Institute Technol.*, 31, 810–811.
Tan, R.T. (2008). Visibility in bad weather from a single image, *Proceedings of the IEEE Conference on Computer Vision and Pattern Recognition*, Anchorage, AK, USA.
Wang, Y.-K. and Fan, C.-T. (2014). Single image defogging by multiscale depth fusion, *IEEE Trans. Image Process.*, 23(11), 4826–4837.
Zeki, S. (1993). *A Vision of the Brain*, J. Wiley and Sons, Eds. Wiley-Blackwell.
Zhang, B. and Zhao, J. (2017). Hardware implementation for real-time haze removal, *IEEE Trans. VLSI Syst.*, 25(3), 1188–1192.
Zhu, Q., Mai, J., and Shao, L. (2015). A fast single image haze removal algorithm using color attenuation prior, *IEEE Trans. Image Process.*, 24(11), 3522–3533.

7 DISCLOSURE STATEMENT

THE authors declare no conflict of interest.

8 NOTES ON CONTRIBUTORS

Yao-Liang Chung (M'12) received the B.S. degree in electrical engineering (first in his class) from Chung Yuan Christian University, Chung Li, Taiwan, in 2004, and the M.S. and Ph.D. degrees in communication engineering from National Taiwan University, Taipei, Taiwan, in 2006 and 2012, respectively.

From 2012 to 2016, he was with the faculty of the Department of Communication Engineering, National Taipei University (NTPU), New Taipei City, Taiwan. Since 2016, he has been on the faculty of the Department of Communications, Navigation and Control Engineering, National Taiwan Ocean University (NTOU), Keelung City, Taiwan, where he is currently an Associate Professor. His current research interests include green information and communications technologies, wireless and cellular networks, artificial intelligence and data analytics, deep learning and deep reinforcement learning, and performance evaluation.

Dr. Chung was the recipient of the Best Master Thesis Award and the Best Ph.D. Dissertation Award of the Institute of Information and Computing Machinery (ACM Taipei/Taiwan Chapter) for his M.S. and Ph.D. theses, respectively; the Excellent Advisor Award of NTPU for his excellent teaching performance in 2015; the Ministry of Science and Technology's Outstanding Young Scholar Research Project Award in 2016; the 6th, 7th, and 8th Excellent Research Awards of the College of Electrical Engineering and Computer Science, NTOU, respectively; the Best Paper Award of the Fourth IEEE International Conference on Future

Generation Communication Technologies, of the 15th IEEE Wireless Telecommunications Symposium, of the Fifth IEEE International Conference on Future Generation Communication Technologies, and of the 12th International Conference on Digital Information Management; the Outstanding Youth Electrical Engineer Award of the Chinese Institute of Electrical Engineering in 2017.

He served as the General Chair of the Seventh International Conference on the Applications of Digital Information and Web Technologies and of the 11th IEEE International Conference on Digital Information Management. He is currently an Associate Editor of the Journal of Intelligent and Fuzzy Systems and the Autosoft Journal. He is a member of Phi Tau Phi Scholastic Honor Society and is also a Senior Member of the International Engineering and Technology Institute.

Hung-Yuan Chung (S'85-M'89-SM'11/FIET'11) received the B.S. degree from National Taiwan Ocean University (NTOU), Taiwan, Republic of China, in 1975 (with the highest honors), and the M.S. degree and Ph.D. degree all in Electrical Engineering from the National Cheng Kung University (NCKU) in 1982 and 1987, respectively. He was with the second division of the Chung Shang Institute of Science Technology (CSIST) from 1977-1984, and with the Mechanical Engineering department of the NCKU in 1984. Since August 1987, he has been with the faculty of the Electrical Engineering department at National Central University (NCU) where he is now a Distinguished Professor.

His extensive research interests and directions involve systems theory and cybernetics, intelligent control, fuzzy logic and neural network applications, bio-medical engineering applications and bio-informatics. He is responsible for the Lab of Intelligent Dynamical Systems at NCU. He has developed and conducted 50+ projects financially supported by the National Science Council (NSC) of the Republic of China (ROC) and folk enterprise since 1989. More recently, he has been interested in service robotics, and analysis of bio-dynamic model. His previous research has resulted in over 350+ publications including 300+ referred journal and conference papers, as well as 50+ technical reports. He also has one ROC Invention Patent. He has also been supervising about 126 graduate students as yet including 10 PhD and 107 MS graduated students and they are holding various important positions in academia, industry, governmental research institutions and folk enterprise, respectively.

He was awarded as Distinguished Professor with tenure in 2010, and received Outstanding Research Award of NCU in recognition of his academic contributions in 2009, 2008, 2007, and 2005, respectively. He was also awarded Outstanding Electrical Engineering Professor from the Chinese Institute of Electrical Engineering (CIEE), Kaohsiung Branch in 2009, Meritorious Service Award of the CIEE in 2004, and Outstanding Electrical Engineer, Kaohsiung Branch in 2003. He got the grade A awards of the NSC of the ROC ten times for accomplishments and contributions of his significant research results.

He also actively joined various Professional Societies and Associations. In International Professional Society, he was a Member of the IEEE from1985 till now, and is currently a Senior Member. He is also a Member of the IEEE Industrial Electronics Society, IEEE Computational Intelligence Society, IEEE Systems, Man, and Cybernetics Society, and a Member of the International Association of Engineers (IAENG), Hong Kong. He was a member of the Institution of Engineering and Technology (IET), United Kingdom and elected to Fellow of the IET in 2011. In National Professional Society, he has been a Permanent Member of the Chinese Institute of Engineers (CIE), Taiwan since 2003, and has been a Permanent Member of the CIEE, Taiwan since 1984.

He has been involving in Professional Service for 30+ years. He has served as a member of organizing committee or technical program committee for many international prestigious conferences sponsored by the IEEE and the IET under different capacities. He has been appointed the committee member of International Advisory Board of Journal of Engineering Research Kuwait University, of IASTED on Biomedical Engineering (Canada) since 2013. In journal editorships, he has served as an Associate Editor of IEEE Transactions on Fuzzy Systems, IEEE Transactions on Neural Network and Learning Systems, Neural Computing & Applications, Journal of Systems Science and Control Engineering (Taylor and Francis), WSEAS Transactions on Systems and Control (SCI), Journal of Applied Mathematics (Hindawi), Journal of Control Science and Engineering (Hindawi), Guest Editor of the IET Systems Biology, Journal of Neurocomputing (SCI, Elsevier), Journal of Intelligent and Fuzzy Systems since 2013, International Journal of Fuzzy Systems since 2012; a Member of Editorial Board of Computer Technology Application, David Publications; a member of Editorial Board of Advances in Fuzzy Sets and Systems, Pushpa Publishing House India; a Member of Editorial Board of Pure Mathematics, Hans Publishers, U.S.A. (2011); a Member of Editorial Board of ISRN Applied Mathematics Hindawi Publisher (2010); a Member of Editorial Advisory Board of The Open Automation and Control Systems Journal, Bentham Science Publishers Ltd. U.S.A. (2008); Editor of Electrical Engineering Communication of the CIEE (1999-2003).

He also served as the reviewer of various Transactions of the IEEE Society a lot, such as Industrial Electronics, Systems, Man and Cybernetics: Part B, Circuits and Systems Part I, Fuzzy Systems, Automatic Control, and so on. Additionally, in public service, he currently serves as Evaluates Committee Member of Executive Yuan Public Works Committee, and Examination Officer Committee Member of Examination Yuan of the ROC.

Yu-Shan Chen received the M.S. degree in electrical engineering from the National Central University, Taiwan, R.O.C., in 2013. She research interests include image processing, robotic control and intelligent control theory applications.